IFT–P.018/99
MADPH–99–1105
February 1999

Strong Interaction Effects in Stop Pair Production at e^+e^- Colliders

Manuel Drees[1] and Oscar J.P. Éboli[1,2]
[1] *Instituto de Física Teórica , Universidade. Estadual Paulista, Rua Pamplona 145, São Paulo, SP 01405-900, Brazil*
[2] *Department of Physics, University of Wisconsin, Madison, WI 53706, USA*

Abstract

We discuss perturbative and non–perturbative strong interaction effects in the pair production of stop squarks ($\tilde{t}_1$) at e^+e^- colliders. Events with an additional hard gluon allow to detect or exclude $\tilde{t}_1\tilde{t}_1^*$ production even in scenarios with very small mass splitting between $\tilde{t}_1$ and an invisible lightest supersymmetric particle (LSP). Such events can also help to establish that $\tilde{t}_1$ transforms as a triplet under $SU(3)_C$. We also carefully study non–perturbative $\tilde{t}_1$ fragmentation, which is currently not well understood: not only is the $\tilde{t}_1$ fragmentation function not known very well, but also there are ambiguities in the algorithm employed to model fragmentation. We present numerical results both for CERN LEP–183 and for a proposed future e^+e^- collider operating at center–of–mass energy $\sqrt{s} = 500$ GeV.

1) Introduction

The lighter scalar top (stop) mass eigenstate $\tilde{t}_1$ is likely to be the lightest squark [1]. In models where supersymmetry breaking is communicated to the superpartners of the known SM particles at some energy well above the weak scale, renormalization group effects reduce the soft mass of the stops compared to those of other squarks. In addition, after the spontaneous breakdown of the electroweak $SU(2) \times U(1)_Y$ symmetry, $SU(2)$ doublet and singlet stops mix, leading to a further reduction of the mass $m_{\tilde{t}_1}$ of the lighter eigenstate. In fact, $\tilde{t}_1$ might even be the lightest charged sparticle. It is therefore actively being searched for at both $p\bar{p}$ [2] and e^+e^- [3, 4] colliders. In this article we focus on $\tilde{t}_1\tilde{t}_1^*$ production at existing and future e^+e^- colliders.

Unlike the other candidates for the lightest charged superparticle, sleptons and the lighter chargino mass eigenstate $\tilde{\chi}_1^\pm$, $\tilde{t}_1$ has strong interactions. Stop pairs can thus be produced in association with a hard gluon. Events of this type can help to overcome Standard Model backgrounds to stop production in scenarios where $\tilde{t}_1$ decays into a lightest neutralino $\tilde{\chi}_1^0$ and a quark, if $\tilde{\chi}_1^0$ is invisible (stable or long–lived) and $m_{\tilde{t}_1} - m_{\tilde{\chi}}$ is small. In such cases the emission of a hard gluon can increase the total visible energy as well as the total missing transverse momentum, helping to discriminate between $\tilde{t}_1\tilde{t}_1^*$ events and backgrounds from two–photon reactions. Once $\tilde{t}_1$ has been discovered, one will also want to study its properties. Events with an additional hard gluon will then be crucial in establishing the color charge of $\tilde{t}_1$.

If $m_{\tilde{t}_1} < m_b + m_{\tilde{\chi}_1^\pm}, m_t + m_{\tilde{\chi}}$, $\tilde{t}_1$ is expected to be quite long–lived [5]. It will then fragment into a "stop meson", which is a spin–1/2 particle, plus a fragmentation jet prior to its decay. This is a non–perturbative process, and hence not well understood. In fact, the very concept of fragmentation is somewhat ill–defined for massive particles: whereas one massless parton can fragment into two collinear massless partons while conserving energy and momentum, a massive particle cannot fragment into another particle with equal (or larger) mass and a second, massless particle with nonvanishing energy. This does not pose much of a problem in the calculation of single–particle inclusive cross sections, through which fragmentation functions are usually defined, but it leads to ambiguities in the implementation of fragmentation in event generator programs. This is of special importance in scenarios with small $\tilde{t}_1$–$\tilde{\chi}_1^0$ mass splitting, where the fragmentation jets may contribute the bulk of the visible energy.

Since non–perturbative $\tilde{t}_1$ fragmentation occurs even if no hard gluon is emitted, we begin by discussing this process in the simple case of $e^+e^- \to \tilde{t}_1\tilde{t}_1^*$. We introduce three different fragmentation schemes, which differ in the precise definition of the fragmentation (scaling) variable x, and/or in the algorithm used to ensure overall energy–momentum conservation. These three algorithms lead to quite different stop energy distributions after fragmentation when used naively with the same fragmentation function. On the other hand, these differences become quite small if the parameter of the fragmentation function is adjusted such that the mean stop "meson" energy is the same in all three scenarios.

In Sec. 3 we discuss events where one hard gluon is emitted. We give an explicit expression for the differential cross section in a form that is easily implementable in an event generator. We then demonstrate, using a parton–level simulation, that the possibility of emitting a hard gluon allows to discover or rule out $\tilde{t}_1$ even for very small mass splitting to the LSP. To this end we employ a set of cuts modeled on the OPAL analysis [4]. These cuts also greatly reduce the sensitivity to the details of $\tilde{t}_1$ fragmentation. We also present a second analysis for a future e^+e^- collider operating at center–of–mass energy $\sqrt{s} = 500$ GeV, as an example of the type of analysis one might perform to determine the color charge of $\tilde{t}_1$. In this case the cross

section after cuts does depend on the details of fragmentation, but the resulting ambiguity in the prediction is much smaller than the perturbatively calculable contribution. Finally, Sec. 4 is devoted to a brief summary and conclusions.

2) Fragmentation

We begin our analysis with a discussion of $\tilde{t}_1$ fragmentation. We will model it using the Peterson *et al.* fragmentation function [6]:

$$D_{\tilde{t}}(x) = \frac{1}{N} \frac{1}{x\left(1 - \frac{1}{x} - \frac{\epsilon_{\tilde{t}}}{1-x}\right)^2} \quad , \tag{1}$$

where the single free parameter $\epsilon_{\tilde{t}}$ is expected to scale as the inverse of the square of the stop mass

$$\epsilon_{\tilde{t}} = \frac{\epsilon}{m^2_{\tilde{t}_1}}, \tag{2}$$

with $\epsilon \sim 0.1$ to 0.5 GeV^2. $D_{\tilde{t}}$ has to satisfy the "stop number conservation" condition $\int_{x_{\rm min}}^1 dx\; x D_{\tilde{t}}(x) = 1$, where $x_{\rm min}$ is the kinematic minimum of x. This leads to

$$N(x_{\rm min}) = \frac{\pi}{4\sqrt{\epsilon_{\tilde{t}}}} - \frac{1}{2}\log\frac{(1-x_{\rm min})^2}{\epsilon_{\tilde{t}}} + 1 - \frac{1}{2(1-x_{\rm min})} + \mathcal{O}(\sqrt{\epsilon_{\tilde{t}}}) \quad . \tag{3}$$

Fragmentation functions are usually defined through differential single–particle inclusive cross sections. In the simple case of leading order stop pair production, $e^+e^- \to \tilde{t}_1\tilde{t}_1^*$, the stop energy prior to fragmentation is fixed* to $\sqrt{s}/2$, so that

$$\frac{d\sigma}{dQ} \propto D_{\tilde{t}}(x) \quad . \tag{4}$$

Unfortunately the choice of Q, and consequently of the associated fragmentation variable x, is somewhat ambiguous for massive particles. It can be the energy E of the stop "meson" $\tilde{t}_M$ after fragmentation, in which case

$$x = x_E \equiv \frac{E_{\tilde{t}_M}}{E_{\tilde{t}_1}} = \frac{2E_{\tilde{t}_M}}{\sqrt{s}} \quad ; \tag{5}$$

or one could choose the absolute value of the 3–momentum $\vec{k}$,

$$x = x_k \equiv \frac{\left|\vec{k}_{\tilde{t}_M}\right|}{\left|\vec{k}_{\tilde{t}_1}\right|} = \frac{2\left|\vec{k}_{\tilde{t}_M}\right|}{\beta\sqrt{s}} \quad , \tag{6}$$

where $\beta = \sqrt{1 - 4m^2_{\tilde{t}_1}/s}$. The second identities in eqs. (5) and (6) hold only for the simple case of $2 \to 2$ kinematics. Occasionally the fragmentation variable is also defined through the "light cone variable" $(E + |\vec{k}|)/2$. This will give results intermediate between the other two choices, so we focus on definitions (5) and (6) here.

*We ignore initial state radiation in our analysis. It can reduce the total cross section by $\sim 20\%$ [7], but will not change most kinematical distributions very much, which are the main emphasis of this work.

A second ambiguity is related to the fact that a massive (s)quark cannot fragment into a hadron of equal or greater mass and one (or more) massless parton(s) without violating energy and/or momentum conservation, if all particles are on–shell. It is therefore not obvious how to introduce fragmentation functions, defined through inclusive cross sections as in eq. (4), into event generator programs that attempt to describe all (relevant) properties of events. We have implemented two different classes of algorithms that ensure energy and momentum conservation at the level of the global event. For simplicity we always model the "fragmentation jet" as a single massless parton collinear with the parent stop.

The first class of algorithms is based on rescaling the 3–momenta of *all* particles in the final state by some overall factor, after the stops have been fragmented. The value of this factor is calculated for each event through iteration, by requiring that all final particles are on–shell and that their energies in the e^+e^- center–of–mass (cms) frame add up to $\sqrt{s}$. These algorithms require that the 3–momenta of all particles after fragmentation, but before rescaling, add up to zero (in the e^+e^- cms frame); overall 3–momentum conservation is then ensured throughout the rescaling process. This means that the fragmentation step itself always has to fix the 3–momentum of the fragmentation jet, even if the fragmentation variable is defined through the stop energy as in eq. (5). In other words, this fragmentation prescription "locally" conserves 3–momentum, but violates energy. Overall ("global") energy conservation is then restored through the rescaling procedure, which not only changes (reduces) the 3–momenta of all particles in the final state but also gives rise to a flow of energy between different parts of the event. This class of algorithms is similar to that employed for the fragmentation of heavy quarks in the ISAJET event simulation package [8]. It can be combined with either definition (5) or (6) of the fragmentation variable; we will call the two resulting algorithms I_E and I_k, respectively.

Note that the sum of the square of the 4–momenta of a stop "meson" and its associated fragmentation jet after rescaling exceeds $m^2_{\tilde{t}_1}$ in the prescriptions I_E and I_k. In other words, one implicitly assumes that the stop squarks were produced slightly off–shell when implementing fragmentation.[†] Our second algorithm makes this explicit, by directly generating a distribution in the squared (off–shell) mass m^2 of the produced stop squarks:

$$m^2(x) = m^2_{\tilde{t}_1} + 2E^2_{\tilde{t}_1}(1-x)\left(1 - \sqrt{1 - \frac{m^2_{\tilde{t}_1}}{E^2_{\tilde{t}_1}}}\right) \quad , \tag{7}$$

where x is distributed according to the fragmentation function $D_{\tilde{t}}(x)$ of eq. (1), and $E_{\tilde{t}_1}$ is the energy of *on–shell* stops, as generated during the calculation of the stop production matrix element. The form (7) has been obtained by writing the stop 4–momenta prior to and after fragmentation as $(E_{\tilde{t}_1}, \vec{k})$ and $(xE_{\tilde{t}_1}, \vec{k}')$, respectively, with $\vec{k}'$ being parallel to $\vec{k}$. One then requires that the difference of these two 4–momenta is light–like (for a massless fragmentation jet), and that the stop meson has mass $m_{\tilde{t}_1}$. This allows to express m^2 as a function of $E_{\tilde{t}_1}$ and $\vec{k}$. In the last step one replaces these quantities by the energy and 3–momentum of on–shell $\tilde{t}_1$; this can be regarded as a one–step iteration. Had we instead defined the stop "meson" 4–momentum as $(E', x\vec{k})$, i.e. tried to implement definition (6) in this scheme via a one–step iteration, the second term on the r.h.s. of eq. (7) would have to be multiplied by an

[†]The matrix elements for stop production are nevertheless computed assuming $\tilde{t}_1$ and $\tilde{t}_1^*$ to be on–shell, so as to reproduce the correct *inclusive* $\tilde{t}_1\tilde{t}_1^*$ production cross section, in accordance with QCD factorization theorems. The same apparent contradiction is built into all QCD fragmentation or parton shower programs we know of.

additional factor $\sqrt{1 - m^2_{\tilde{t}_1}/E^2_{\tilde{t}_1}}$. However, we will stick to the ansatz (7) for scheme II here, since the difference between the definitions (5) and (6) of the scaling variable will be explored by comparing the results of schemes I_E and I_k.

Once the masses of $\tilde{t}_1$ and $\tilde{t}^*_1$ have been generated according to eq. (7), the energies and 3–momenta of all particles in the final state have to be recomputed, using new limits of phase space as appropriate for the increased stop masses. In so doing, care has to be taken to generate kinematic quantities that "correspond" to those used (prior to fragmentation) to compute the squared matrix element for stop production, which enters the event weight. This can be accomplished as follows. Assume the phase space is parameterized by a set of kinematic quantities q_i, $i = 1, \ldots, N$. The kinematic limits of q_i are determined by $\sqrt{s}$, by the masses of $\tilde{t}_1$ and $\tilde{t}^*_1$, and (for $i \neq 1$) by the values of $q_1, \ldots, q_{i-1}$. An event can then be characterized by a set of dimensionless numbers $r_i \in [0, 1]$, so that $q_i = q_{i,\min} + r_i(q_{i,\max} - q_{i,\min})$; the r_i can be viewed as the random numbers used by a Monte Carlo integration of phase space. The correspondence between "fragmented" and "unfragmented" events can then be ensured by using the same set $\{r_i\}$ when regenerating all 4–momenta after fragmentation, only modifying the kinematical limits to accommodate increased stop squark masses for the "fragmented" events. Once the 4–momenta of the off–shell squarks have been generated in this way, fragmentation itself can be treated as the (collinear) decay of a particle with mass m into a second particle with mass $m_{\tilde{t}_1}$ and a massless parton.

This second algorithm has both advantages and disadvantages. On the positive side, there is no need for iterative rescaling of 3–momenta after fragmentation; however, as described in the previous paragraph, all 4–momenta do need to be recomputed, allowing for different (virtual) $\tilde{t}_1$ and $\tilde{t}^*_1$ masses. Another potential advantage is that, although the ansatz (7) has been designed to emulate a conventional fragmentation function using definition (5) of the scaling variable, it could easily be converted into a fully Lorentz invariant fragmentation scheme, since the mass m^2 is a Lorentz invariant. This would be more difficult to accomplish in both variants of scheme I, which are based on non Lorentz covariant quantities (energies and 3–momenta). On the other hand, at least as implemented using eq. (7), scheme II does not have a smooth limit as $m_{\tilde{t}_1} \to 0$. Eq. (7) then always gives $m^2 = 0$, independent of x, leaving the 4–momenta of the fragmentation products undefined. In contrast, in the massless limit schemes I_E and I_k both approach the same scheme (corresponding to independent fragmentation, again as in ISAJET [8]), where no rescaling of 3–momenta is required.

Rather than working with variable (virtual) stop squark masses and fixed stop "meson" mass, one might also consider keeping the stop squark masses fixed at $m_{\tilde{t}_1}$, but varying the stop meson masses. This would also allow to implement energy–momentum conservation without any rescaling. However, there are several problems with such a scheme. Energy–momentum conservation would force the "mesons" to be lighter than the squarks, whereas flavored D and B mesons are heavier than c and b quarks. Also, a continuous stop meson energy distribution would correspond to a continuous stop meson mass spectrum as well. For these reasons we will not explore this alternative any further.

In Figs. 1a,b we compare results for our three fragmentation schemes. We have chosen a parameter set of current interest, $\sqrt{s} = 183$ GeV and $m_{\tilde{t}_1} = 80$ GeV. The solid, long dashed and short dashed curves refer to schemes I_k, I_E and II, respectively. We have taken $\tilde{t}_1$ to be a pure $SU(2)$ doublet ($\theta_{\tilde{t}} = 0$ in the notation of refs. [7, 9]), but this only affects the overall normalization of the curves. We have also included "soft and virtual" QCD corrections [9], defined through an infrared cut–off for emitted gluons of 1 GeV. This ensures that we are only studying events with $2 \to 2$ kinematics; events with additional hard gluon will be discussed

in Sec. 3.

In Fig. 1a we compare the stop "meson" spectra produced by our three schemes. We have taken the same value of ϵ in all three cases, but the resulting spectra clearly differ substantially. The difference between schemes I_E and I_k is fairly easy to understand. Since the produced stop squarks are far from being ultra–relativistic ($\beta \simeq 0.5$), reducing their 3–momenta by some factor x corresponds to a much smaller relative reduction of their total energies, which receive a large (constant) contribution from their mass. As a result, for fixed ϵ scheme I_k leads to a much harder stop "meson" spectrum than scheme I_E does. Except for the steep drop towards the lower kinematical endpoint of the distribution, scheme II falls in between the two variants of scheme I here. The large differences displayed in this figure clearly show that care must be taken when comparing the values of the free parameters of heavy (s)quark fragmentation functions obtained from different event simulation programs, with possibly different implementations of the fragmentation process.

On the other hand, Fig. 1b shows that at least for the simple case of exclusive $\tilde{t}_1\tilde{t}_1^*$ production ($2 \to 2$ kinematics), the differences between fragmentation schemes can largely be absorbed into a change of the value of the parameter ϵ of eq. (2). Here we have chosen ϵ in each scheme such that the average stop meson energy coincides with the prediction of the original Peterson *et al.* function (1); using $\epsilon = 0.5$ GeV^2 and the definition (5) of the scaling variable, it predicts $\langle E_{\tilde{t}_M} \rangle = 89.1$ GeV. Almost no change of ϵ is required in scheme II. On the other hand, in scheme I_E, ϵ has to be reduced to 0.1 GeV^2, while in scheme I_k it has to be increased to 2.0 GeV^2, in order to reproduce the same $\langle E_{\tilde{t}_M} \rangle$. These two values of ϵ differ by a factor of 20!

After this adaptation of ϵ, the three schemes give quite similar results for the stop "meson" spectrum, except near its lower kinematical boundary. However, recall that these schemes ensure energy–momentum conservation only globally. This means that the fragmentation process will change the 4–momenta of partons that seemingly have nothing to do with it. This is actually not as unreasonable as it may sound, since color neutralization in any case connects different partons during hadronization. Furthermore, notice that none of the three schemes reproduces the original Peterson function, shown as the dotted curve, near the upper endpoint of the spectrum. The reason is that, due to the requirements of overall energy–momentum conservation, our schemes allow $E_{\tilde{t}_M} \simeq \sqrt{s}/2$ only if *both* fragmentation variables are close to 1, which is obviously much less likely than having only one of them close to unity. We will see in the next Section that even after adapting the value of ϵ so as to produce the same $\langle E_{\tilde{t}_M} \rangle$, the three schemes lead to somewhat more pronounced differences in events with additional hard gluon.

3) Hard gluon emission

In this Section we discuss the production of a $\tilde{t}_1\tilde{t}_1^*$ pair in association with a hard gluon, $e^+e^- \to \tilde{t}_1\tilde{t}_1^* g$. The gluon can be emitted from either of the two stop lines; in addition, there are diagrams with a $\gamma\tilde{t}_1\tilde{t}_1^* g$ or $Z\tilde{t}_1\tilde{t}_1^* g$ vertex. This process has been treated previously in refs. [9, 10, 11], using parameterizations of phase space that simplify analytical calculations. In contrast, our treatment is geared towards easy implementation in an event generator program. The spin–averaged squared matrix element is

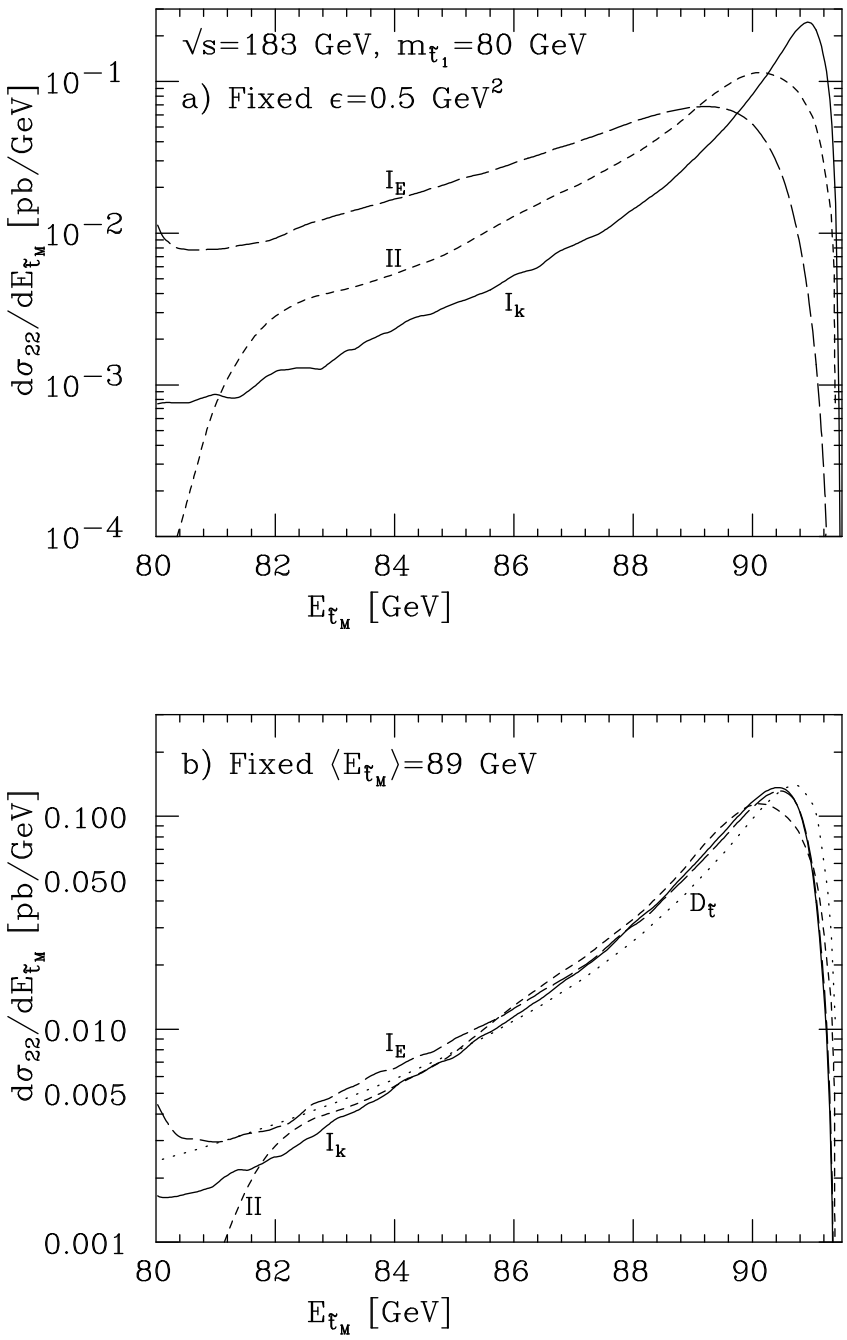

Figure 1: The stop "meson" spectrum as predicted by the three fragmentation schemes described in the text. All three schemes employ the Peterson *et al.* fragmentation function. In a) the same value of the parameter ϵ has been used in all cases, while in b) the value of ϵ has been adjusted so as to reproduce the prediction $\langle E_{\tilde{t}_M} \rangle \simeq 89$ GeV of the original Peterson *et al.* fragmentation function with $\epsilon = 0.5$ GeV^2, using the definition (5) for the scaling variable; this gives $\epsilon = 0.1, 2.0$ and 0.5 GeV^2 for schemes I_E, I_k and II, respectively. The shape of the Peterson *et al.* fragmentation function is shown by the dotted curve.

$$
\begin{aligned}
&\left|\overline{\mathcal{M}}\left(e^+(p_1)\ e^-(p_2) \to \tilde{t}_1(k_1)\ \tilde{t}_1^*(k_2)\ g(q)\right)\right|^2 \\
&= 4\frac{g_s^2 e^4}{s^2}\left(|A|^2+|B|^2\right)\left\{4s - 2m_{\tilde{t}_1}^2\left[\frac{4k_1\cdot p_1\ k_1\cdot p_2 - s\ m_{\tilde{t}_1}^2}{(k_2\cdot q)^2} + \frac{4k_2\cdot p_1\ k_2\cdot p_2 - s\ m_{\tilde{t}_1}^2}{(k_1\cdot q)^2}\right]\right. \\
&\qquad\left. + \frac{k_1\cdot q + k_2\cdot q + k_1\cdot k_2}{k_1\cdot q k_2\cdot q}\left[s\ k_1\cdot k_2 - 2\left(p_1\cdot k_1\ p_2\cdot k_2 + p_2\cdot k_1\ p_1\cdot k_2\right)\right]\right\} \\
&\equiv 4\frac{g_s^2 e^4}{s^2}\left(|A|^2+|B|^2\right)\left|\widetilde{\mathcal{M}}\right|^2 \quad , \qquad (8)
\end{aligned}
$$

where g_s is the strong coupling constant, which we take at scale $\mu = \sqrt{s}$, and e is the QED coupling. The coefficients A and B describe the strength of the effective vector and axial vector couplings, being given by

$$A = q_{\tilde{t}} - \frac{(1-4\sin^2\theta_W)c_{\tilde{t}}}{8\sin^2\theta_W\cos^2\theta_W}\cdot\frac{s}{s-M_Z^2+iM_Z\Gamma_Z} \quad ; \qquad (9a)$$

$$B = \frac{c_{\tilde{t}}}{8\sin^2\theta_W\cos^2\theta_W}\cdot\frac{s}{s-M_Z^2+iM_Z\Gamma_Z} \quad , \qquad (9b)$$

where

$$c_{\tilde{t}} = 2q_{\tilde{t}}\sin^2\theta_W - 2\cos^2\theta_{\tilde{t}} I_{3_{\tilde{t}}} \qquad (10)$$

describes the $Z\tilde{t}_1\tilde{t}_1^*$ coupling [7] with $\theta_{\tilde{t}}$ being the stop mixing angle (the angle between $\tilde{t}_1$ and $\tilde{t}_L$); $q_{\tilde{t}}$ $(= +2/3)$ and $I_{3_{\tilde{t}}}$ $(= +1/2)$ are the $\tilde{t}_1$ charge and $\tilde{t}_L$ weak isospin, respectively.

The cross section can now be expressed in terms of the reduced squared matrix element $\left|\widetilde{\mathcal{M}}\right|^2$ introduced in eq. (8):

$$\sigma(e^+e^- \to \tilde{t}_1\tilde{t}_1^* g) = \frac{\alpha_s\alpha_{em}^2}{\pi s^3}\left(|A|^2+|B|^2\right)\int dE_g\ d\cos\theta_g\ dE_{\tilde{t}}\ d\phi_{\tilde{t}}\ \left|\widetilde{\mathcal{M}}\right|^2 \quad . \qquad (11)$$

Here, E_g and $E_{\tilde{t}}$ are the energies of the gluon and of $\tilde{t}_1$ in the e^+e^- cms frame, θ_g is the angle between the gluon and the direction of the positron beam, and $\phi_{\tilde{t}}$ determines the direction of the $\tilde{t}_1$ 3–momentum, as follows. We choose the frame where the gluon's 3–momentum is given by

$$\vec{q} = E_g(0, \sin\theta_g, \cos\theta_g) \quad , \qquad (12)$$

i.e. the integration over the polar angle of the gluon has been performed explicitly in eq. (11), yielding a factor of 2π. The $\tilde{t}_1$ 3–momentum is then given by

$$\vec{k}_1 = \sqrt{E_{\tilde{t}}^2 - m_1^2}(\sin\phi_{\tilde{t}}\sin\alpha, \cos\theta_g\cos\phi_{\tilde{t}}\sin\alpha + \sin\theta_g\cos\alpha, \cos\theta_g\cos\alpha - \sin\theta_g\cos\phi_{\tilde{t}}\sin\alpha), \qquad (13)$$

where

$$\cos\alpha = \frac{s - 2\sqrt{s}(E_g+E_{\tilde{t}}) + 2E_gE_{\tilde{t}} + m_1^2 - m_2^2}{2E_g\sqrt{E_{\tilde{t}}^2 - m_1^2}} \qquad (14)$$

is the angle between $\tilde{t}_1$ and the gluon, which is fixed for given E_g and $E_{\tilde{t}}$. Note that we have allowed for different $\tilde{t}_1$ and $\tilde{t}_1^*$ masses m_1 and m_2 in eq. (14), as required for the implementation of our fragmentation scheme II discussed in the previous section. However, for the purpose

of computing event weights $m_1 = m_2 = m_{\tilde{t}_1}$ should be used. The $\tilde{t}_1^*$ 3–momentum can now trivially be computed from eqs. (12)–(14) as $\vec{k}_2 = -\vec{k}_1 - \vec{q}$.

Finally, the limits of phase space integration, again allowing for different $\tilde{t}_1$ and $\tilde{t}_1^*$ masses, are:

$$E_g \in [E_g^{\min}, \frac{s-(m_1+m_2)^2}{2\sqrt{s}}] \ ; \tag{15a}$$

$$\cos\theta_g \in [-1,1] \ ; \tag{15b}$$

$$\phi_{\tilde{t}} \in [0, 2\pi] \ ; \tag{15c}$$

$$E_{\tilde{t}} \in [E_-, E_+] \ , \tag{15d}$$

where

$$E_\pm = \frac{\sqrt{s}-E_g}{2}\left[1+\frac{m_1^2-m_2^2}{\sqrt{s}(\sqrt{s}-2E_g)}\right] \pm \frac{E_g}{2}\sqrt{\left[1+\frac{m_1^2-m_2^2}{\sqrt{s}(\sqrt{s}-2E_g)}\right]^2 - \frac{4m_1^2}{\sqrt{s}(\sqrt{s}-2E_g)}} \ . \tag{16}$$

Note that the squared matrix element (8) diverges linearly as $E_g \to 0$. This requires the introduction of an infrared cut–off $E_g^{\min}$ in eq. (15a). The same cut–off also appears (logarithmically) in the expression for the "soft + virtual" QCD corrections. Physical quantities do not depend on $E_g^{\min}$, if it is chosen sufficiently small so that events containing a gluon with energy $E_g = E_g^{\min}$ still effectively possess $2 \to 2$ kinematics. We have checked numerically that eqs. (8)–(16) reproduce the "hard" real QCD corrections to the total $\tilde{t}_1\tilde{t}_1^*$ production cross section as given in ref. [9] (and contained implicitly in [7]). Of course, stop fragmentation, as implemented using either of our schemes, does not change the total cross section before cuts.

In the subsequent analysis we have taken into account the $\tilde{t}_1$ decay, which we have assumed to be always into a massless quark* plus an invisible LSP $\tilde{\chi}_1^0$. A first illustration of the impact of both perturbative and non–perturbative strong interaction effects on $\tilde{t}_1\tilde{t}_1^*$ production is shown in Fig. 2, where we plot the total visible energy for $\sqrt{s} = 183$ GeV, $m_{\tilde{t}_1} = 70$ GeV, and $m_{\tilde{\chi}} = 67$ GeV. We have chosen a scenario with very small $\tilde{t}_1$–LSP mass splitting, since in this case strong interaction effects are most important. This is illustrated by the difference between the dotted curve, where all such effects have been switched off, and the other curves. In the absence of strong interaction effects, and before any cuts have been applied, the visible energy spectrum has a triangular shape, centered at $E_q^* \cdot (\sqrt{s}/m_{\tilde{t}_1}) \simeq 7.7$ GeV, where $E_q^* = (m_{\tilde{t}_1}^2 - m_{\tilde{\chi}}^2)/(2m_{\tilde{t}_1})$ is the quark energy in the $\tilde{t}_1$ rest frame. We see that strong interaction effects are expected to nearly double the average visible energy for our choice of sparticle masses.

However, there are significant uncertainties in this prediction, due to our lack of understanding of non–perturbative $\tilde{t}_1$ fragmentation. Different fragmentation schemes using the same fragmentation function can give quite different results, as can be seen by comparing the long and short dashed curves, which are valid for schemes I_E and II, respectively, with $\epsilon = 0.5$ GeV^2. Such a difference is not surprising, given the results of Fig. 1. However, even after adjusting the value of ϵ used in scheme I_E so as to reproduce the average stop "meson" energy predicted by scheme II, which is very close to the value predicted directly from the Peterson

*In models with exact universality of the squark masses at the scale M_X of Grand Unification one expects $\tilde{t}_1$ to dominantly decay into a charm quark [5]; in this case the visible energy could be further degraded by semileptonic decays of the charm (anti)quark. However, there is no compelling reason to assume exact (rather than only approximate) squark degeneracy at M_X. Moreover, $\tilde{t}_1$ decays are independent of the strong interaction effects on $\tilde{t}_1\tilde{t}_1^*$ pair production, which are the main focus of our analysis.

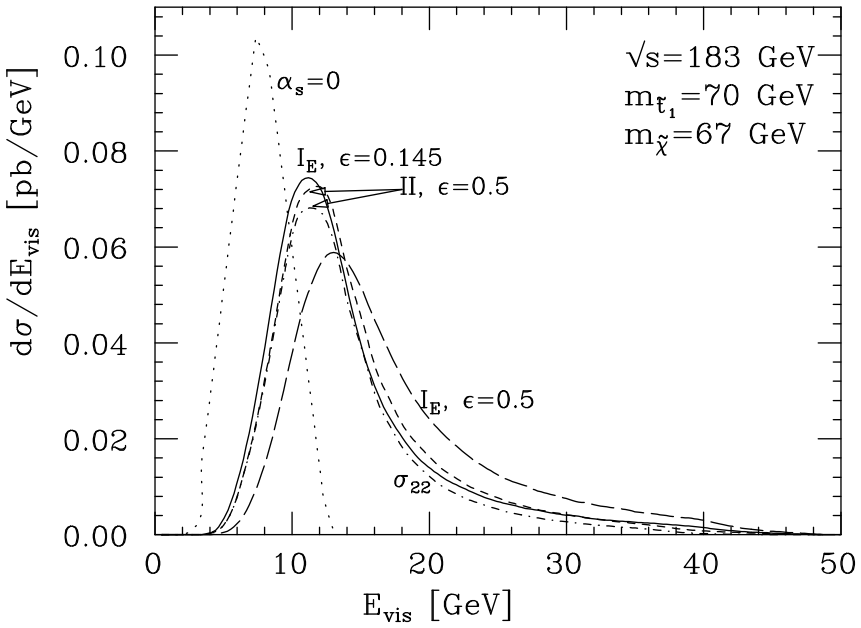

Figure 2: The total visible energy in $e^+e^- \to \tilde{t}_1\tilde{t}_1^*(g)$ events at LEP–183. The dotted curve has been obtained by switching off both perturbative and non–perturbative strong interaction effects, while the dot–dashed curve includes non–perturbative $\tilde{t}_1$ fragmentation but no hard gluon radiation (defined with an infrared cut–off $E_g^{\rm min} = 1$ GeV). The other curves include both perturbative and non–perturbative effects. The labels refer to the fragmentation scheme used, and give the value of the fragmentation parameter ϵ of eq. (2) in units of GeV^2.

et al. fragmentation function, some discrepancies remain. Indeed, the difference between the predictions of scheme $\rm I_E$ with adjusted ϵ parameter (solid curve) and scheme II is comparable in size to the effect of hard gluon radiation, which can be seen by comparing the short dashed and dot–dashed curves; the former shows the full cross section, while the latter is for the $2 \to 2$ contribution only.

One might be tempted to conclude from Fig. 2 that non–perturbative stop fragmentation by itself can release a sufficient amount of visible energy to give a viable signal for $\tilde{t}_1\tilde{t}_1^*$ production even for small $\tilde{t}_1$–LSP mass splittings. However, one should keep in mind that in the absence of hard gluon radiation, the fragmentation products will always be almost back–to–back in the transverse plane, and the $\tilde{t}_1$ decay products are not energetic enough to change this picture. Unfortunately there are large backgrounds to such configurations, even if one requires a substantial transverse momentum imbalance. The main source of backgrounds are two photon processes. They can lead to large (apparent) missing p_T either through semileptonic decays of charm quarks, or through mismeasurement since the energies of the jets are quite low, so that calorimetry becomes rather imprecise. Recent experimental searches [3, 4] therefore discard such back–to–back configurations. This will enhance the importance of signal events containing an additional hard gluon.

This is illustrated in Fig. 3, where we have attempted to incorporate the most important cuts applied by the OPAL collaboration [4] into our parton level event generator. We show the

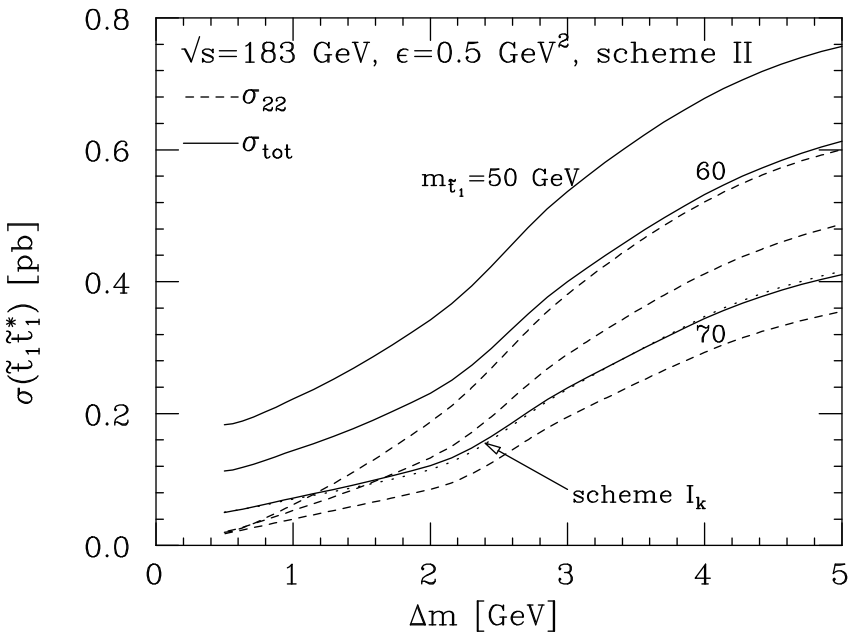

Figure 3: The total inclusive $\tilde{t}_1\tilde{t}_1^*$ cross section at LEP–183 after the cuts (17) have been applied. The solid curves show the full result, while the dashed curves have been computed by switching off hard gluon radiation. For $m_{\tilde{t}_1} = 50$ and 60 GeV, the infrared cut–off has been chosen such that the total cross section before cuts of the $2 \to 2$ contribution reproduces the leading order, $\mathcal{O}(\alpha_s^0)$, prediction; this gives $E_g^{\min} = 5.4$ (1.8) GeV for $m_{\tilde{t}_1} = 50$ (60) GeV. For $m_{\tilde{t}_1} = 70$ GeV this would give a very small value of $E_g^{\min}$, so we have chosen 1.0 GeV instead. Recall that the total result (solid curves) does not depend on $E_g^{\min}$. All curves are for fragmentation scheme II, except the dotted one, which is for scheme I_k.

total inclusive $\tilde{t}_1\tilde{t}_1^*$ cross section at $\sqrt{s} = 183$ GeV after the following cuts have been applied:

$$M_{\rm vis} > 4.0 \text{ GeV} \ ; \tag{17a}$$

$$p_{T,\rm miss} > 4.5 \text{ GeV} \ ; \tag{17b}$$

$$|\cos\theta_{\rm miss}| < 0.9 \ ; \tag{17c}$$

$$\phi_{\rm acop} > 20^\circ \ . \tag{17d}$$

In order to model the geometric acceptance of a typical LEP detector, we have discarded all partons with azimuthal angle $|\cos\theta| > 0.97$ before computing the total visible mass $M_{\rm vis}$ and missing transverse momentum $p_{T,\rm miss}$. The cut (17c) is on the angle of the missing momentum vector with the beam pipe. OPAL also requires that the k_T clustering algorithm [12] with fixed jet resolution parameter $y_{\rm cut}$ produce exactly two jets, and applies cuts on the invariant masses of these jets. However, it is difficult to model such cuts accurately with a parton level event generator. Furthermore, insisting on exactly two jets with given $y_{\rm cut}$ would tend to remove events containing a hard gluon in addition to the $\tilde{t}_1\tilde{t}_1^*$ pair. Therefore, the full set of cuts applied by the OPAL collaboration is not efficient for scenarios with very small $\tilde{t}_1 - \tilde{\chi}_1^0$

mass splitting. We have instead used the k_T clustering algorithm to force the event into a two–jet structure, except for events with less than two partons in the acceptance region of the detector, which we discarded – that is, we kept merging jets until exactly two jets remain. We then applied the cut (17d) on the angle between these two jets in the transverse plane.

The results of Fig. 3 indicate that the emission of a hard gluon should allow to detect or exclude $\tilde{t}_1\tilde{t}_1^*$ pair production even for arbitrarily small $\tilde{t}_1 - \tilde{\chi}_1^0$ mass splitting. The published OPAL limit [4] on $m_{\tilde{t}_1}$ corresponds to a total cross section of 0.13 pb, after the cuts (17) have been applied. This indicates that existing data might allow to exclude, or find evidence for, a $\tilde{t}_1$ nearly degenerate with the LSP up to $m_{\tilde{t}_1} \simeq 60$ GeV for mixing angle $\theta_{\tilde{t}} = 0$. Of course, a complete experimental analysis would be needed to really establish such a bound. We emphasize that an accurate description of hard gluon radiation would be crucial for such an analysis. Leading–log parton shower models, as used in refs. [3, 4], cannot be expected to model this process accurately. The importance of this $2 \to 3$ contribution is illustrated by the dashed curves, where this contribution has been turned off; the cross section after cuts then goes to zero in the limit of vanishing $\tilde{t}_1 - \tilde{\chi}_1^0$ mass difference.

Most results shown in Fig. 3 have been computed using scheme II with $\epsilon = 0.5$ GeV^2. However, the cuts (17) greatly reduce the sensitivity to the details of the fragmentation process. This is illustrated by the dotted curve, which shows the inclusive $\tilde{t}_1\tilde{t}_1^*$ cross section after cuts for $m_{\tilde{t}_1} = 70$ GeV, as predicted using scheme I_k with the *same* value of ϵ. We saw in Fig. 1 that this corresponds to a significantly harder stop "meson" spectrum, *i.e.* much softer fragmentation jets. Nevertheless the predicted cross section is almost the same as that for scheme II. This is due to a somewhat fortuitous cancellation: models with harder fragmentation jets predict a significantly larger cross sections after the cuts (17a,b) have been applied; however, the resulting event then also tends to be more back–to–back, so that a relatively larger number of events is removed by the cut (17d). This weak sensitivity to the details of the fragmentation process has also been noticed in the experimental searches [3, 4], where it was studied by varying the parameter ϵ of the Peterson *et al.* fragmentation function. This result is very welcome, since it almost removes one (potentially large) source of uncertainty of the measured (limit on the) total $\tilde{t}_1\tilde{t}_1^*$ cross section.

As already mentioned in the Introduction, events with an additional hard gluon might also help to determine the color charge of $\tilde{t}_1$.[†] Given the present experimental limits, a definitive analysis of this kind may only be possible at a high energy, high luminosity linear e^+e^- collider (LC)[‡]. Various designs of such colliders are now being studied, with quoted luminosities ranging up to 500 fb^{-1}/yr [13].

Assuming that $\tilde{t}_1$ always undergoes 2–body decay into a light quark and an invisible LSP $\tilde{\chi}_1^0$, the most direct way to determine its color charge is probably through the study of events with 3 or more jets. Notwithstanding, non–perturbative $\tilde{t}_1$ fragmentation can also produce jets. Fortunately these fragmentation jets are expected to be quite soft; perturbative contributions should therefore dominate for sufficiently large jet energies.

This is borne out by Fig. 4, which shows results of an analysis for $\sqrt{s} = 500$ GeV, $m_{\tilde{t}_1} = 150$ GeV, and $m_{\tilde{\chi}} = 100$ GeV. Allowing for the (probably) larger beam holes of future LC detectors

[†]The "3–jet" contribution to the total inclusive cross section for the production of a pair of colored scalars has been calculated in [11]; however, that analysis did not treat fragmentation and decay of the scalars, nor were any cuts applied to reject the background.

[‡]Of course, the discovery of $\tilde{t}_1$ at a hadron collider would immediately prove that it carries a nonvanishing color charge. However, in order to confirm that it belongs to an $SU(3)_C$ triplet one would have to measure both $m_{\tilde{t}_1}$ and the $\tilde{t}_1\tilde{t}_1^*$ production cross section, which may not be easy.

as compared to present LEP detectors, we have discarded all partons with $|\cos\theta| > 0.9$. We then used the k_T clustering algorithm [12] to force the event into a 3–jet structure. Following ref. [14], we demanded that the hardest two jets have energies $E_{\mathrm{jet}_{1,2}} > 15$ GeV, and that the total missing p_T exceeds 35 GeV; this removes most SM backgrounds. Fig. 4 shows the energy spectrum of the third (softest) jet after these cuts.

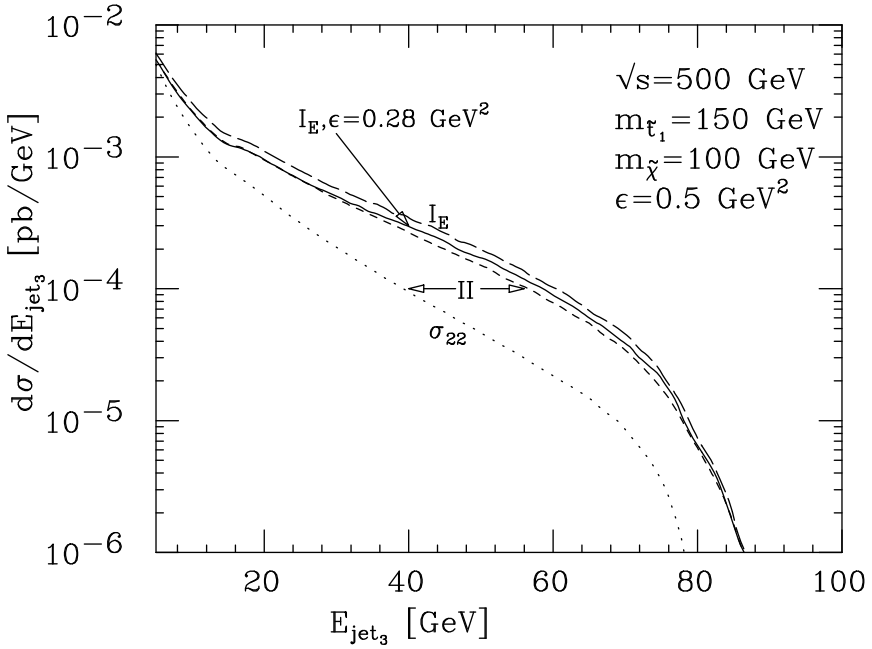

Figure 4: The spectrum of the softest jet produced in $\tilde{t}_1\tilde{t}_1^*$ production at a future linear collider after the cuts described in the text, where the events have been forced into a 3–jet topology using the k_T clustering algorithm. The small shoulder at $E_{\mathrm{jet}_3} = 15$ GeV is caused by the cut on the energies of the two hardest jets. The dotted curve shows the result in the absence of hard gluon radiation, as predicted using fragmentation scheme II, while the other three curves show the total inclusive cross section. They differ in the fragmentation scheme and/or in the value of the fragmentation parameter ϵ, as indicated.

The dotted curve shows the contribution of events without hard gluon (defined through an IR cut–off $E_g^{\min} = 5$ GeV), while the other three curves include contributions from both $2 \to 2$ and $2 \to 3$ processes. We see that for $E_{\mathrm{jet}_3} > 15$ GeV, the cross section is dominated by perturbative contributions. However, a significant dependence on the details of non–perturbative $\tilde{t}_1$ fragmentation remains even in this region. We saw in Fig. 1 that for a given value of ϵ, scheme I_E predicts a softer stop "meson" spectrum, *i.e.* harder fragmentation jets, than scheme II does. It is therefore not surprising that scheme I_E predicts the third jet to be somewhat more energetic. However, some difference between the predictions from these two schemes remains even if the value of ϵ is adjusted to reproduce the same average stop "meson" energy. After this adjustments the two schemes make very similar predictions for $E_{\mathrm{jet}_3} \leq 30$ GeV, where most events still have an effective $2 \to 2$ kinematics. Nevertheless, our different methods to ensure overall energy–momentum conservation still give somewhat different predictions for

$E_{\rm jet_3} > 30$ GeV, where most events contain a quite energetic gluon.

These differences are partly due to the fact that we force all events into a 3–jet structure, so that the gluon is often merged with (some of) the fragmentation products. This source of dependence on the fragmentation scheme can probably be reduced if a different jet definition is used. On the other hand, the two schemes also predict a somewhat different gluon energy spectrum even prior to any jet merging. We therefore expect that some dependence on the fragmentation scheme will remain for all jet definitions. Of course, for the parameters chosen in Fig. 4, the large number of $\tilde{t}_1\tilde{t}_1^*$ pair events ($\sim 65,000$ signal events after cuts for an integrated luminosity of 500 fb^{-1}) should also allow to study various aspects of non–perturbative $\tilde{t}_1$ fragmentation in detail. Moreover, since the differences between the predictions of our fragmentation schemes are far smaller than the overall contribution of events containing hard gluons, even our current level of understanding of non–perturbative $\tilde{t}_1$ fragmentation would suffice to ascertain with a high degree of confidence that $\tilde{t}_1$ is indeed a color triplet.

4) Summary and Conclusions

We have examined the effects of both perturbative and non–perturbative strong interactions on $\tilde{t}_1\tilde{t}_1^*$ production at current and future e^+e^- colliders. The latter manifests itself in $\tilde{t}_1$ fragmentation into a stop "meson", while the former gives rise to events containing a hard gluon in addition to the stop squarks.

Non–perturbative $\tilde{t}_1$ fragmentation has been discussed in some detail in Sec. 2, with particular emphasis on the conceptual ambiguities of the fragmentation of heavy partons. These ambiguities are largest for beam energies somewhat, but not far, above the pair production threshold, *i.e.* precisely in the region where squark production can best be studied at e^+e^- colliders. They include not only the definition of the fragmentation (scaling) variable, but also the algorithm used to ensure overall energy–momentum conservation. The scaling variable can be defined either through the energy or through the absolute value of the 3–momentum (or through some combination thereof). These two quantities coincide for massless partons, and also for massive partons in the infinite momentum frame where QCD factorization theorems are often formulated. However, they can differ greatly for massive partons in the laboratory frame, where event generators are needed to describe the data. We also introduced two different schemes to guarantee overall energy and momentum conservation after fragmentation. The first scheme is based on the re–scaling of all 3–momenta, and is quite similar to algorithms employed in multi–purpose event generators like ISAJET. In the second scheme, which bears some resemblance to algorithms often used to model perturbative parton showering, one explicitly generates a distribution in the virtuality of the produced squarks. We saw that these schemes can lead to quite different results when applied naively to the same fragmentation function. However, at least in the simple case of exclusive $\tilde{t}_1\tilde{t}_1^*$ production, *i.e.* in the absence of hard gluon radiation, most of these differences can be absorbed in a redefinition of the parameter(s) of the fragmentation function.

Events containing hard gluons have been studied in Sec. 3. After giving explicit expressions for the corresponding fully differential cross section, we showed that such events should allow to extend the sensitivity of e^+e^- collider experiments to scenarios with arbitrarily small mass splitting between $\tilde{t}_1$ and the lightest superparticle $\tilde{\chi}_1^0$, which we assume to be invisible. The gluon by itself can produce a sufficient amount of visible energy, and of missing transverse momentum and acoplanarity, to discriminate between signal and background even if $\tilde{t}_1$ decays

release almost no visible energy. We found that the cuts used to suppress Standard Model backgrounds also reduce the sensitivity of the predicted cross section to the details of $\tilde{t}_1$ fragmentation to a negligible level. Hard gluon radiation had previously been found [15] to increase the sensitivity of hadron colliders to $\tilde{t}_1\tilde{t}_1^*$ pair production in scenarios with small stop–LSP mass splitting. However, that analysis treated gluon radiation only in leading logarithmic approximation (through the parton shower algorithm of ISAJET), rather than through exact matrix elements. Moreover, scenarios with mass splitting below 20 GeV still remained undetectable in hadronic collisions.

We have also indicated how an analysis of 3–jet events from $\tilde{t}_1\tilde{t}_1^*$ pair production at a future linear collider operating at high energy and high luminosity can be used to determine the color charge of $\tilde{t}_1$. In this case some sensitivity to $\tilde{t}_1$ fragmentation remains after cuts.

Our numerical results include both real and virtual ordinary QCD corrections. However, we did not include initial state radiation, nor did we include corrections from loops including gluinos, *i.e.* "SUSY QCD corrections" [10, 16]. Both effects mostly change the overall normalization of the $\tilde{t}_1\tilde{t}_1^*$ production cross section, leaving the shapes of the distributions studied here almost unchanged.[§] The total cross section also depends on the $\tilde{t}_L - \tilde{t}_R$ mixing angle $\theta_{\tilde{t}}$, which we set to zero in our numerical examples.

The numerical analyses presented here are by no means an exhaustive list of the effects of strong interactions on stop production at e^+e^- colliders. For example, strong interactions will play a role in measurements of the stop and LSP masses from $\tilde{t}_1\tilde{t}_1^*$ events. This is true in particular in scenarios with small stop–LSP mass splitting, where a large fraction of the total visible energy can come from non–perturbative $\tilde{t}_1$ fragmentation or hard gluon radiation, as illustrated in Fig. 2. Even if this mass splitting is quite large, the extracted values of these masses could be shifted by several GeV if the analysis is not designed such as to minimize these effects.

While the other very short–lived squarks are not expected to undergo non–perturbative fragmentation, hard gluon radiation will occur with equal relative frequency for all squark flavors. The cross section given in Sec. 3 can easily be adapted to the production of other squarks by changing the relevant electroweak couplings. Many SUSY models predict first and second generation squarks to be closely degenerate in mass; moreover, $SU(2)$ doublet squarks might undergo quite complicated cascade decays even if they are lighter than the gluino. One will then need a more sophisticated analysis to experimentally determine their color charges. The effect of hard gluon radiation on squark mass measurements in such a scenario [14] also needs to be investigated. On the other hand, since $\tilde{t}_1$ might well be very long–lived compared to the time scale of strong interactions in spite of being very heavy in relation to the QCD scale Λ, it might even provide us with a unique tool to study non–perturbative aspects of the hadronization process. Analyses of squark pair production at e^+e^- colliders can thus not only yield valuable information on these (as yet hypothetical) new particles, but might even improve our understanding of some basic aspects of strong interactions.

Acknowledgements

MD acknowledges financial support from FAPESP (Brazil). OJPE gratefully acknowledges the hospitality of the Phenomenology Institute of the University of Wisconsin. This work was sup-

[§]Events where a hard photon is radiated down one of the beam pipes will have significantly reduced visible energy. However, the cross section for such events is quite small, unless the collider operates at energies far above the stop threshold.

ported in part by the University of Wisconsin Research Committee with funds granted by the Wisconsin Alumni Research Foundation, by the U.S. Department of Energy under grant DE-FG02-95ER40896, by Conselho Nacional de Desenvolvimento Científico e Tecnológico (CNPq), by Fundação de Amparo à Pesquisa do Estado de São Paulo (FAPESP), and by Programa de Apoio a Núcleos de Excelência (PRONEX).

References

[1] J. Ellis and S. Rudaz, Phys. Lett. **B128**, 248 (1983).

[2] DØ collab., S. Abachi *et al.*, Phys. Rev. Lett. **76**, 2222 (1996); C.M. Holck for the CDF collab., FERMILAB-CONF-98-208-E, contributed to the *29th International Conference on High-Energy Physics (ICHEP 98)*, Vancouver, Canada, 23-29 July 1998.

[3] ALEPH collab., R. Barate *et al.*, Phys. Lett. **B413**, 431 (1997), and Phys. Lett. **B434**, 189 (1998) [hep–ex/9810028]; DELPHI collab., P. Abreu *et al.*, Eur. Phys. J. **C6**, 385 (1999).

[4] OPAL collab., K. Ackerstaff *et al.*, Eur. Phys. J. **C6**, 225 (1999) [hep–ex/9808026].

[5] K. Hikasa and M. Kobayashi, Phys. Rev. **D36**, 724 (1987).

[6] C. Peterson, D. Schlatter, I. Schmitt, and P.M. Zerwas, Phys. Rev. **D27**, 105 (1983).

[7] M. Drees and K. Hikasa, Phys. Lett. **B252**, 127 (1990).

[8] F.E. Paige, S.D. Protopopescu, H.A. Baer, and X.R. Tata, hep–ph/9810440, and references therein.

[9] W. Beenakker, R. Höpker, and P.M. Zerwas, Phys. Lett. **B349**, 463 (1995) [hep–ph/9501292].

[10] A. Arhrib, M. Capdequi–Peyranere and A. Djouadi, Phys. Rev. **D52**, 1404 (1995) [hep–ph/9412382].

[11] K. Hikasa and J. Hisano, Phys. Rev. **D54**, 1908 (1996) [hep–ph/9603203].

[12] S. Catani, Yu.L. Dokshitzer, M. Olsson, G. Turnock, and B.R. Webber, Phys. Lett. **B269**, 432 (1991).

[13] ECFA/DESY LC Physics Working Group, E. Accomando *et al.*, Phys. Rep. **299**, 1 (1998) [hep–ph/9705442].

[14] J.L. Feng and D.E. Finnell, Phys. Rev. **D49**, 2369 (1994) [hep–ph/9310211].

[15] H.A. Baer, J. Sender, and X.R. Tata, Phys. Rev. **D50**, 4517 (1994) [hep–ph/9404342].

[16] H. Eberl, A. Bartl, and W. Majerotto, Nucl. Phys. **B472**, 481 (1996) [hep–ph/9603206].